Reversible Electric-Field-Driven Magnetic Domain-Wall Motion

Kévin J. A. Franke,[1] Ben Van de Wiele,[2] Yasuhiro Shirahata,[3] Sampo J. Hämäläinen,[1] Tomoyasu Taniyama,[3] and Sebastiaan van Dijken[1,*]

[1]*NanoSpin, Department of Applied Physics, Aalto University School of Science, P.O. Box 15100, FI-00076 Aalto, Finland*

[2]*Department of Electrical Energy, Systems and Automation, Ghent University, Ghent B-9000, Belgium*

[3]*Materials and Structures Laboratory, Tokyo Institute of Technology, 4259 Nagatsuta, Midori-ku, Yokohama 226-8503, Japan*

(Received 22 August 2014; revised manuscript received 19 December 2014; published 3 February 2015)

Control of magnetic domain-wall motion by electric fields has recently attracted scientific attention because of its potential for magnetic logic and memory devices. Here, we report on a new driving mechanism that allows for magnetic domain-wall motion in an applied electric field without the concurrent use of a magnetic field or spin-polarized electric current. The mechanism is based on elastic coupling between magnetic and ferroelectric domain walls in multiferroic heterostructures. Pure electric-field-driven magnetic domain-wall motion is demonstrated for epitaxial Fe films on $BaTiO_3$ with in-plane and out-of-plane polarized domains. In this system, magnetic domain-wall motion is fully reversible and the velocity of the walls varies exponentially as a function of out-of-plane electric-field strength.

DOI: 10.1103/PhysRevX.5.011010 Subject Areas: Condensed Matter Physics, Magnetism

I. INTRODUCTION

Domain walls in ferromagnetic thin films or nanowires are conventionally driven by magnetic fields or spin-polarized electric currents [1–10]. The velocity of magnetic domain walls varies with the driving force and various material properties (magnetic anisotropy, damping constant, saturation magnetization, etc.), which give rise to several dynamic regimes [11]. In the thermally activated creep regime, domain-wall motion depends sensitively on the disorder-induced pinning energy barrier and the depinning field [12]. This notion has led to various demonstrations of electric-field control over the pinning strength and velocity of magnetic domain walls via voltage-induced changes of magnetic anisotropy. Examples include the use of dielectric gates or ferroelectric films to manipulate the magnetic anisotropy via charge modulation or band shifting [13–20]. Other promising methods utilize strain coupling to piezoelectric materials [21,22] or electric-field-induced ionic diffusion [23]. Voltage-controlled domain-wall gates and traps based on these concepts provide new prospects for magnetic logic and memory technologies. In all instances, the magnetic domain walls are driven by a magnetic field or electric current and the velocity of the walls is altered by an electric-field effect on the magnetic anisotropy. Besides, electric-field-induced magnetic domain-wall deformations [24] and magnetic switching via lateral domain-wall motion [25] have been demonstrated in piezoelectric-magnetostrictive heterostructures with competing anisotropies.

Magnetoelectric coupling between a ferroelectric material and a ferromagnetic film in multiferroic heterostructures has been extensively studied during the last decade, and various interaction mechanisms have been identified as promising routes toward electric-field control of magnetism [26–29]. In exchange- and strain-coupled systems, direct correlations between the polarization direction within ferroelectric domains and locally induced magnetic anisotropies have been demonstrated [30–36]. Multiferroic heterostructures with lateral anisotropy modulations are characterized by strong pinning of magnetic domain walls onto narrow ferroelectric domain boundaries [37]. This robust coupling effect forces the magnetic domain walls to follow their ferroelectric counterparts when the latter are displaced in an applied electric field, thus providing a new way to drive magnetic domain walls by pure electrical means. In our previous work, we studied electric-field-induced magnetic switching via lateral domain-wall motion in polycrystalline CoFe films that were strain coupled to ferroelastic a_1 and a_2 domains of a $BaTiO_3$ substrate [38]. Because of partial strain transfer during film growth and in-plane orientation of ferroelectric polarization in these structures, complex domain patterns evolved in an out-of-plane electric field and accurate control over domain-wall motion could not be obtained.

Here, we report on the ability to reversibly and deterministically drive magnetic domain walls by an electric field only. Full electric-field control over the magnetic

*sebastiaan.van.dijken@aalto.fi

domain-wall velocity in the absence of a magnetic field or spin-polarized electric current is demonstrated using epitaxial Fe films on single-crystal $BaTiO_3$ substrates with alternating in-plane (*a* domains) and out-of-plane (*c* domains) ferroelectric polarization. The magnetic domain walls of the Fe film are strongly pinned onto the *a*-*c* boundaries of the $BaTiO_3$ substrate by abrupt changes in the symmetry and strength of magnetic anisotropy. The back-and-forth motion of a ferroelectric *a*-*c* boundary and a pinned magnetic domain wall is realized by the application of positive and negative out-of-plane voltage pulses. In our proof-of-concept experiments, the domain-wall velocity is varied over 5 orders of magnitude by adjusting the electric-field strength. Micromagnetic simulations indicate that near-180° transverse magnetic domain walls can be stabilized in magnetic nanowires on top of $BaTiO_3$. The spin structure and strong elastic pinning of such domain walls to *a*-*c* boundaries are sustained up to high driving velocities.

II. SAMPLE FABRICATION AND CHARACTERIZATION

Fe films with a thickness of 20 nm are grown onto single-crystal $BaTiO_3$ substrates with a thickness of 0.5 mm using molecular beam epitaxy at 300 °C. Regular ferroelectric *a* and *c* domains are imprinted into the Fe layer upon cooling through the Curie temperature of $BaTiO_3$ at $T_C = 120$ °C, which coincides with a cubic-to-tetragonal structural phase transition. At room temperature, the Fe film is capped by 5 nm of Au to prevent oxidation during sample characterization. Growth of Fe onto the (001)-oriented $BaTiO_3$ substrates is epitaxial with an Fe[110]//$BaTiO_3$[100] crystal alignment in the film plane [39].

The ferromagnetic domains and domain walls of the Fe film are imaged using a magneto-optical Kerr-effect microscope. Magnetization reversal on top of the ferroelectric *a* and *c* domains is characterized for in-plane magnetic fields. Electric-field-driven magnetic domain-wall motion in zero magnetic field is analyzed in the same microscope by applying out-of-plane voltage pulses across the $BaTiO_3$ substrate. In these experiments, the backside of the sample is contacted by double-sided copper tape and wire bonding to the metallic Fe/Au layer is used to create the top electrode. Bias-voltage pulses are generated by a bipolar power supply with the Fe/Au top electrode contacted to ground. The strength of the electric field is varied from 0.5 to 8 kV/cm. Magnetic domain-wall displacements are determined from Kerr-microscopy images that are recorded prior to and immediately after the application of a voltage pulse.

III. EXPERIMENTAL RESULTS

At room temperature, the tetragonal $BaTiO_3$ substrate consists of domains with in-plane (*a* domain) and out-of-plane (*c* domain) ferroelectric polarization. Rotation of the polarization at the domain boundaries coincides with an abrupt change of the $BaTiO_3$ in-plane lattice structure: The unit cell of *a* domains in the (001)-oriented surface is rectangular with a tetragonality of 1.1%, and the in-plane lattice of *c* domains is cubic. The ferroelectric polarization and lattice tetragonality of the *a* domains are oriented perpendicular to the domain walls. The regular modulations of lattice symmetry in the $BaTiO_3$ substrate are reflected by the magnetic anisotropy of the Fe film whose magnetoelastic component is induced via strain transfer at the heterostructure interface and inverse magnetostriction. Because of the negative magnetostriction constant of Fe, the easy axis of magnetization on top of ferroelectric *a* domains is oriented perpendicular to the ferroelectric polarization and thus parallel to the domain wall, while the two magnetic easy axes on top of *c* domains are aligned at 45°. Figure 1(a) depicts the experimental configuration. Here, a schematic illustration of an *a* and *c* domain in the $BaTiO_3$ substrate is combined with a Kerr-microscopy image of the magnetic microstructure in the Fe film for

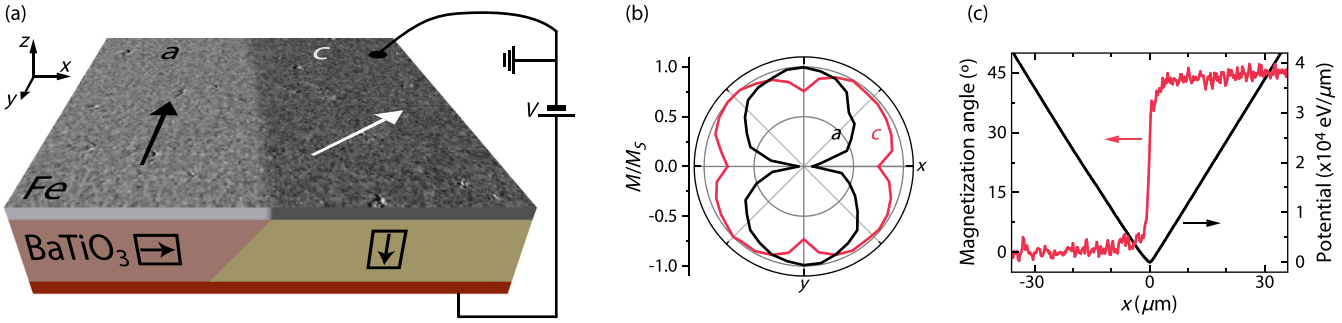

FIG. 1. (a) Schematic illustration and Kerr-microscopy image of the Fe/$BaTiO_3$ heterostructure with ferroelectric *a* and *c* domains. Arrows indicate the direction of ferroelectric polarization in the $BaTiO_3$ substrate and the direction of magnetization in the Fe film in zero magnetic field. Measurements of electric-field-driven magnetic domain-wall motion are conducted by contacting the Fe/Au layer to ground and applying bias-voltage pulses to the back side of the $BaTiO_3$ substrate. (b) Polar plots of the remanent magnetization on top of the *a* domain (black line) and *c* domain (red line). (c) Measured profile of the magnetic domain wall in (a) (red line) and the calculated pinning potential (black line).

zero magnetic field. Full angular analyses of the local remanent magnetization [polar plots in Fig. 1(b)] confirm the twofold and fourfold symmetry of magnetic anisotropy on top of the ferroelectric *a* and *c* domains. The corresponding magnetic anisotropy strengths, as determined from fits to local hard-axis hysteresis curves, are $K_a = 2 \times 10^4$ J/m^3 and $K_c = 1 \times 10^4$ J/m^3.

A. Magnetic domain-wall pinning

The abrupt change in symmetry and strength of magnetic anisotropy on top of $BaTiO_3$ *a*-*c* domain walls produces narrow and straight anisotropy boundaries inside the Fe film. Magnetic domain walls are strongly pinned by these anisotropy boundaries. This pinning effect can be understood by considering a lateral displacement of a pinned magnetic domain wall away from a ferroelectric boundary. Such a movement would cause a misalignment between the local magnetization and the easy anisotropy axes, thereby enhancing the total magnetic anisotropy energy of the system. The pinning potential can be calculated if the magnetization profile of the domain wall and the symmetry and strength of the magnetic anisotropy on either side of the anisotropy boundary are known (see the Appendix for details). Figure 1(c) shows the magnetization profile of a pinned magnetic domain wall on top of a ferroelectric *a*-*c* boundary as measured by Kerr microscopy. Also shown is the pinning potential, which is calculated using the wall profile and the experimental values for K_a and K_c. The minimum of the pinning potential is located on top of the ferroelectric *a*-*c* boundary ($x = 0$), and the magnetic anisotropy energy increases sharply when the magnetic domain wall is displaced. We note that this analysis of magnetic domain-wall pinning must be considered as a first-order approximation, not taking into account possible deformations of the magnetic domain-wall profile and assuming a perfectly abrupt ferroelectric boundary. The latter simplification is justified by experimental results and theoretical calculations indicating a ferroelastic domain-wall width of only 2–5 nm in $BaTiO_3$ [40–42], which is more than one order of magnitude smaller than the width of magnetic domain walls in 20-nm-thick Fe films.

Strong magnetic domain-wall pinning is confirmed by the Kerr-microscopy data of Fig. 2. In the images, magnetization reversal in the Fe film for a magnetic field perpendicular to the domain wall is shown. The wall that separates the two ferromagnetic domains is fully immobilized by elastic coupling to the underlying ferroelectric *a*-*c* boundary in the $BaTiO_3$ substrate. The magnetizations of both domains reverse independently. The magnetic contrast on top of the ferroelectric *a* domain (lower part of the images) changes gradually, indicating coherent magnetization rotation. This behavior is explained by the perpendicular alignment of the easy anisotropy axis and the in-plane magnetic field. Magnetization reversal on top of the ferroelectric *c* domain (upper part of the images) proceeds by coherent rotation

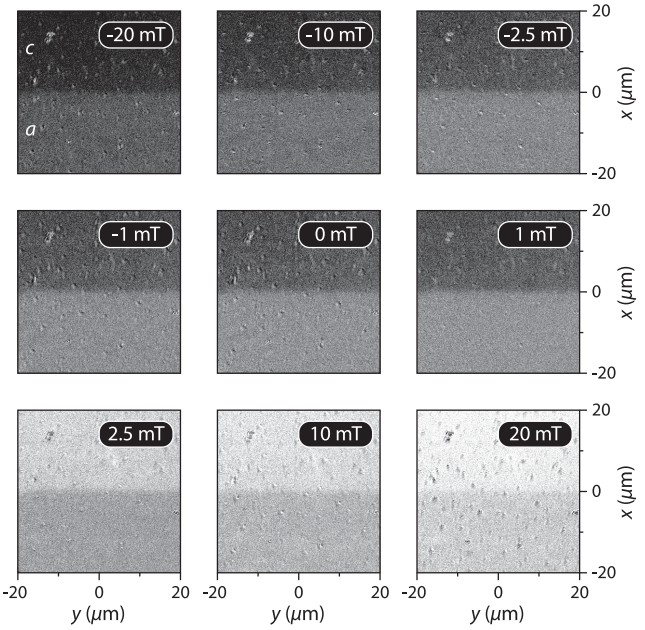

FIG. 2. Kerr-microscopy images of magnetization reversal in an Fe film on top of a $BaTiO_3$ substrate. The in-plane magnetic field and the axis of magneto-optical Kerr-effect contrast are aligned perpendicular to the domain wall.

and abrupt switching at a magnetic field of 2.5 mT. In this case, the magnetic field is oriented along one of the hard axes of the cubic magnetic anisotropy. While the spin rotation of the magnetic domain wall changes with applied magnetic-field strength, its position remains firmly fixed on top of the ferroelectric boundary in the $BaTiO_3$ substrate.

B. Electric-field-driven magnetic domain-wall motion

Domain boundaries in the $BaTiO_3$ substrate can be moved by the application of an electric field. The concurrent motion of magnetic anisotropy boundaries and their pinning potential in an elastically coupled ferromagnetic film can be utilized to drive magnetic domain walls by pure electrical means. Reversible motion of an electric-field-driven magnetic domain wall is demonstrated in Fig. 3. The Kerr-microscopy images show the remanent magnetic microstructure of the Fe film on top of a $BaTiO_3$ substrate with a ferroelectric *a*-*c* domain boundary. Reversible motion of the ferroelectric boundary and the pinned magnetic domain wall is achieved by the application of out-of-plane electric-field pulses [see Fig. 1(a)]. If the electric field is aligned along the direction of ferroelectric polarization in the *c* domain (negative bias voltage), the *c* domain grows at the expense of the neighboring *a* domain by lateral wall motion toward the bottom of the images. A positive bias voltage, on the other hand, shrinks the *c* domain by moving the ferroelectric boundary and pinned magnetic domain wall back up. Strong elastic coupling necessitates that the magnetic domain wall in the Fe film

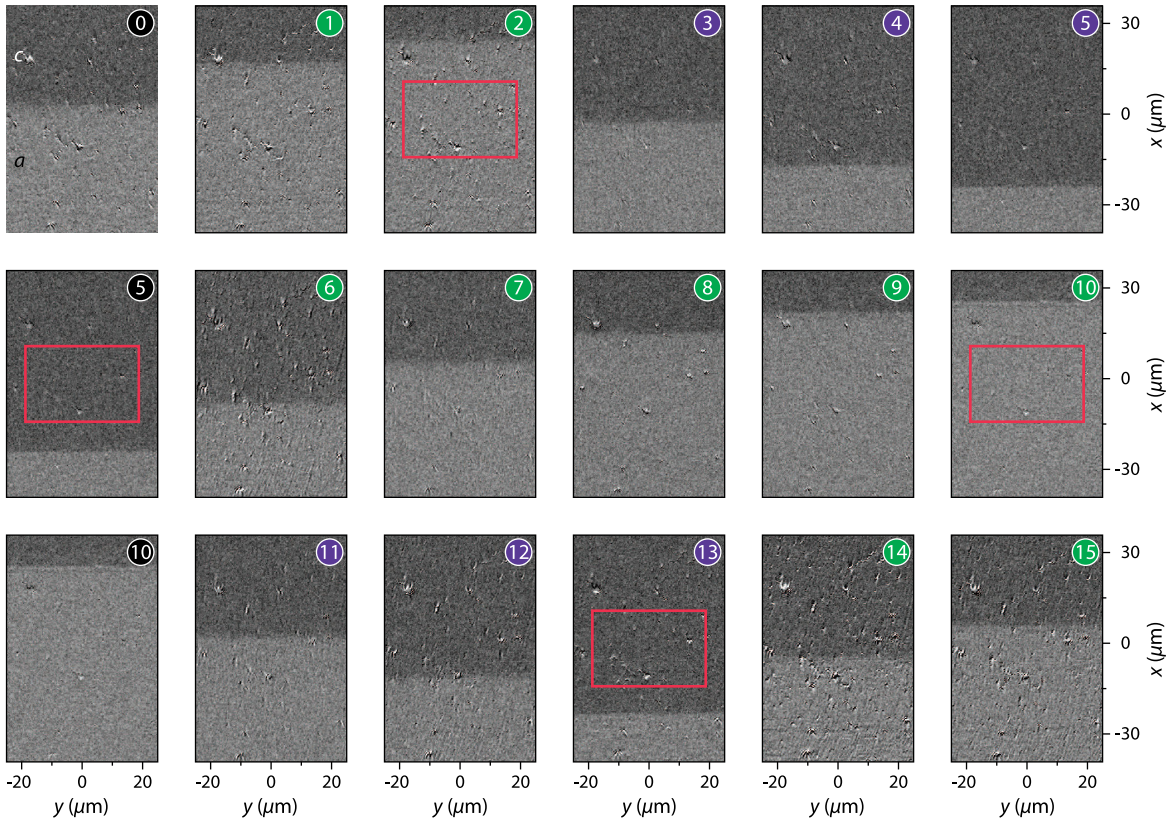

FIG. 3. Kerr-microscopy images illustrating the motion of a magnetic domain wall in an Fe film during the application of positive (green circles) and negative (violet circles) voltage pulses across the $BaTiO_3$ substrate. Black circles indicate that no voltage pulse is applied between two consecutive images. The pulse strength is $|V| = 100$ V, which corresponds to an electric field of $|E| = 2$ kV/cm. The red boxes denote an area for which magnetic hysteresis curves are measured after electric-field-driven magnetic domain-wall motion [see Fig. 4(b)].

closely follows the displacement of the ferroelectric domain boundary.

The position of the magnetic domain wall as a function of the number of electric-field pulses is plotted in Fig. 4(a). The velocity of the magnetic domain wall decreases when it departs from its original position by several micrometers. This feature is characteristic for ferroelastic domain-wall motion in $BaTiO_3$ and other ferroelectric materials [43,44]. The built-in restoring force that the *a*-*c* domain wall experiences is caused by a repulsive interaction between ferroelastic walls in the $BaTiO_3$ substrate. Since the magnetic domain wall in the Fe film is strongly pinned onto the ferroelastic boundary, its electric-field-driven motion is intrinsically linked to the ferroelectric subsystem. Isolation of a single domain wall in multiferroic heterostructures would eliminate the dependence of domain-wall motion on sample position.

Figure 4(b) shows magnetic hysteresis curves from the same sample area (red boxes in Fig. 3) after the repeated back-and-forth motion of the magnetic domain wall. The direction of the in-plane magnetic field in these measurements is perpendicular to the domain wall. The data indicate an alternation of magnetic anisotropy from uniaxial (when the entire area is located on top of the ferroelectric *a* domain) to biaxial (when the underlying ferroelectric domain is of *c* type). The strength and symmetry of the magnetic anisotropy, however, are preserved upon repeated domain-wall cycling in an applied electric field. Thus, contrary to other electric-field effects [13–25], the mechanism discussed in this paper does not alter the magnitude of magnetic anisotropy. Instead, the magnetic domain wall in the Fe film follows the sideways motion of an anisotropy boundary that is induced by a ferroelectric *a*-*c* domain wall in the $BaTiO_3$ substrate, while the distinctive magnetic anisotropies on top of the *a* and *c* domains are conserved.

The dependence of the average domain-wall velocity on electric-field strength is recorded by adjusting the duration of the electric-field pulse (Δt) to the electric-field strength (E), so that accurate measurements of domain-wall displacement (Δx) could be obtained by Kerr microscopy. The velocity of elastically coupled magnetic and ferroelectric domain walls is subsequently inferred from $v(E) = \Delta x/\Delta t$. The results are presented in Fig. 5. An exponential increase of domain-wall velocity with increasing electric field is obtained, which is characteristic of thermally

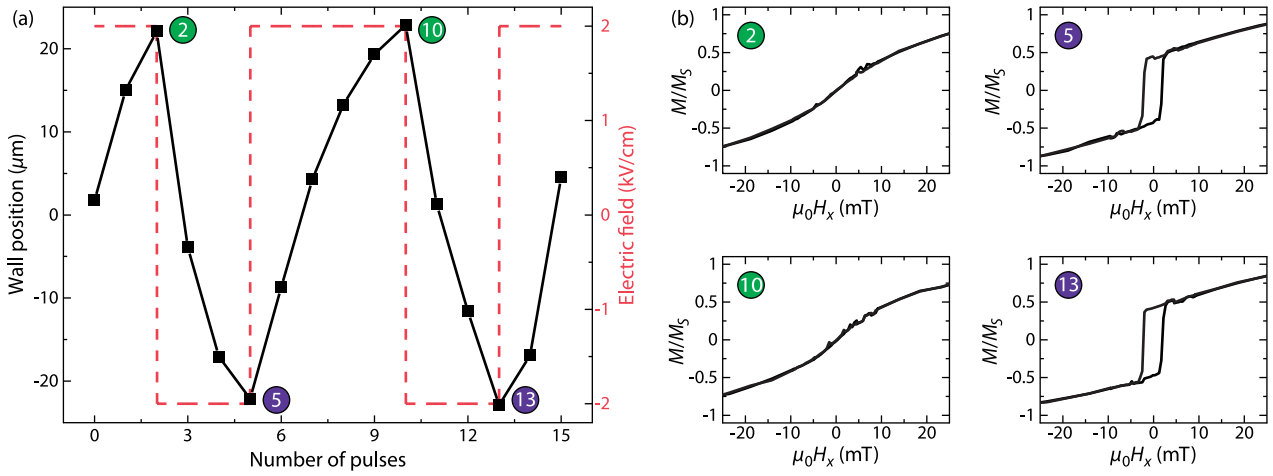

FIG. 4. (a) Magnetic domain-wall position in the Fe film after the application of a series of positive and negative electric-field pulses across the $BaTiO_3$ substrate. The polarity and strength of the electric field are indicated by a dashed red line. The numbers correspond to the measurements in Fig. 3. (b) Magnetic hysteresis curves for a selected sample area (red boxes in Fig. 3). The data evidence that alternations between uniaxial (*a* domain) and biaxial (*c* domain) magnetic anisotropy during the back-and-forth motion of the magnetic domain wall are reproducible.

assisted depinning of ferroelectric domain walls in the strong-pinning regime [43]. The velocity of the magnetic domain wall in the Fe film can be controlled over 5 orders of magnitude in the current experiments. While this result is very promising, the maximum recorded velocity falls short of the anticipated upper limit for electric-field-driven ferroelectric domain walls. The main reason is the thickness of the $BaTiO_3$ substrate (0.5 mm), which requires the use of large bias voltages. An extension of this proof-of-concept investigation to higher domain-wall velocities could be attained by replacing the $BaTiO_3$ substrate by a thinner ferroelectric crystal. Such a configuration would allow for the application of short pulses of large electric field at low bias voltage. Since the dynamics of electric-field-driven magnetic domain-wall motion is mainly governed by the ferroelectric subsystem, the upper bound of fast domain-wall motion is set by the ferroelectric material. Studies on domain-wall dynamics in $BaTiO_3$ crystals indicate that wall velocities up to 1000 m/s can be achieved at room temperature [45]. In magnetic nanowires, magnetostatic shape anisotropy might cause depinning of magnetic domain walls at very high speeds, which will be discussed in the next section.

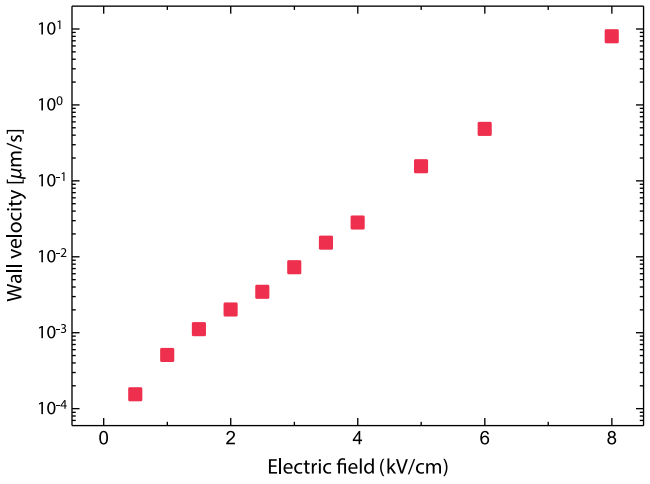

FIG. 5. Magnetic domain-wall velocity as a function of applied electric field.

IV. MICROMAGNETIC SIMULATIONS

Micromagnetic simulations are performed to study the structure and motion of pinned magnetic domain walls in patterned nanowires. The simulations are conducted with the graphics-processing-unit-based micromagnetic simulator MuMax [46,47]. To closely mimic strain coupling in the $Fe/BaTiO_3$ system, experimental values for the magnetic anisotropy on top of ferroelectric *a* and *c* domains are used (i.e., $K_a = 2 \times 10^4$ J/m^3 and $K_c = 1 \times 10^4$ J/m^3). Other input parameters for the Fe film include a saturation magnetization of $M_S = 1.7 \times 10^6$ A/m, an exchange constant of $K_{ex} = 2.1 \times 10^{-11}$ J/m, and a damping constant of $\alpha = 0.01$. An infinitely long and 200-nm-wide nanowire with a thickness of 5 nm and successive *a* and *c* domains of length 3.2 μm is considered. Using periodic boundary conditions along the nanowire axis, the computational area is restricted to one set of *a* and *c* domains. Finite difference cells of size $3.125 \times 3.125 \times 5$ nm are used to discretize the geometry. Motion of the anisotropy boundary at a velocity v_{AB} is implemented by shifting the anisotropy boundary over a distance of one cell ($\delta x = 3.125$ nm) every $\delta t = \delta x / v_{AB}$.

The simulations reveal that patterning of ferromagnetic films into nanowire geometries offers additional degrees of freedom for the engineering of robust and strongly pinned

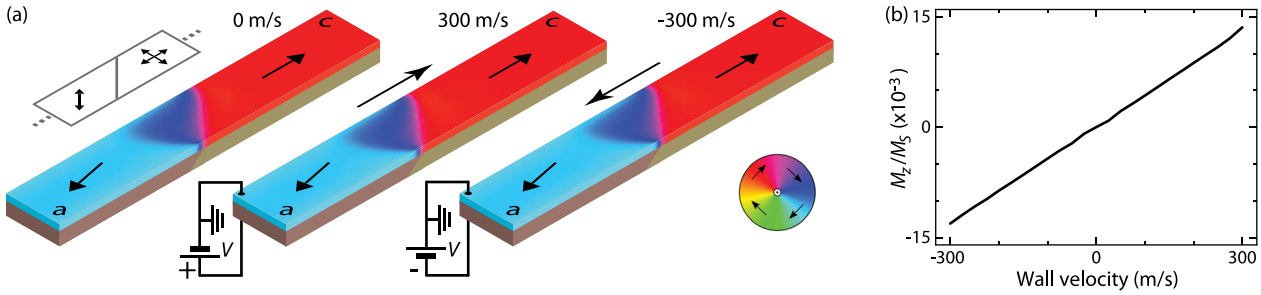

FIG. 6. Micromagnetic simulations of magnetic domain-wall motion in a 200-nm-wide and 5-nm-thick Fe wire. The schematic in the upper left corner indicates the easy magnetic anisotropy axes in the nanowire. The shape anisotropy of the wire stabilizes a near-180° transverse magnetic domain wall in zero magnetic field, which is strongly pinned by an abrupt anisotropy boundary on top of a ferroelectric *a*-*c* domain wall. Fast motion of the anisotropy boundary in both directions results in an equally fast displacement of the transverse magnetic domain wall with only minor deformations of the internal wall structure. The data in (a) illustrate the magnetic structure of the nanowire at rest and for $v_{AB} = +300$ m/s and $v_{AB} = -300$ m/s. The evolution of a small out-of-plane magnetization component with increasing domain-wall velocity is shown in (b).

magnetic domain walls. For example, despite the 45° angle between the magnetic anisotropy axes on top of the ferroelectric *a* and *c* domains, near-180° transverse magnetic domain walls can be stabilized in magnetic nanowires because of competing magnetostatic shape anisotropy, as shown in Fig. 6. At rest and zero applied magnetic field, a transverse domain wall is formed and pinned onto the magnetic anisotropy boundary between the *a* and *c* domains. Fast motion of the anisotropy boundary to the right or left by 300 m/s does not depin or drastically alter the spin structure of the magnetic domain wall. Only a small out-of-plane magnetization component develops as a function of wall velocity [Fig. 6(b)], which is reminiscent of the pre-Walker-breakdown behavior of magnetic-field or current-driven domain-wall motion [7]. At even larger driving velocities, the magnetic domain wall depins from the anisotropy boundary when out-of-plane magnetization tilting reaches a threshold value. The critical depinning velocity depends sensitively on competing exchange, magnetostatic, and anisotropy energies. In micromagnetic simulations, we observe the following trends: An increase of the magnetic anisotropy strength suppresses magnetization tilting, and, as a result, larger depinning velocities are obtained. In contrast, a reduction of the magnetic nanowire width or an increase of its thickness leads to domain-wall depinning at lower velocities. Importantly, robust pinning with negligible domain-wall deformation is sustained up to several hundreds of meters per second for a large parameter space (film thickness, wire width, and anisotropy strength), which is comparable to fast magnetic-field or current-driven domain-wall motion in magnetic nanowires [3,6,9,10].

As shown in this paper, elastic coupling of a ferromagnetic film to a ferroelectric layer with straight domain walls introduces 1D pinning potentials whose locations can be controlled by an electric field. In addition, randomly distributed pinning potentials due to material disorder (impurities, grain boundaries, etc.) or patterning imperfections (e.g., edge roughness) will also be present in experimental systems. To estimate the influence of such disorder on electric-field-driven magnetic domain-wall motion, we simulate the same nanowire geometry as in Fig. 6(a) for a polycrystalline ferromagnetic film. In the simulations, weak exchange coupling between grains with a nominal size of 20 nm is mimicked by reducing the exchange stiffness at the grain boundaries [48]. An exchange-stiffness reduction of 25% results in pinning potentials with a depth of about 1 eV, which corresponds to experimental results [49–51]. Although the introduction of random disorder reduces the critical depinning velocity by about 10%, it does not affect the motion of electric-field-driven magnetic domain walls below the depinning threshold. This insensitivity to noncontrollable disorder can be considered as an important advantage over magnetic-field or current-driven domain-wall dynamics in the thermally activated creep regime. In the latter cases, domain-wall depinning is a stochastic process and the average domain-wall velocity varies strongly with random pinning potentials. The simulation data also suggest that the electric-field-driving mechanism is not limited to epitaxial heterostructures with low defect densities. Similar effects can be anticipated for polycrystalline ferromagnetic films, provided that strain coupling to a ferroelectric layer and inverse magnetostriction are strong enough to establish full domain-pattern transfer.

V. POWER CONSUMPTION

Electric-field-driven magnetic domain-wall motion provides a low-power alternative for magnetic devices because of negligible current flow through the ferroelectric part of multiferroic heterostructures. The energy advantage over current-driven domain-wall motion in magnetic nanowires can be estimated by comparing relevant material parameters and device geometries. For current-driven magnetic domain-wall motion via the spin-transfer torque (STT) effect, large current densities (J) of the order of 10^{12} A/m^2 are required.

Consequently, resistive Joule heating is the main source of power losses. The power consumption of this driving mechanism can be estimated by $P_{\mathrm{STT}} = \rho_{\mathrm{FM}} V_{\mathrm{FM}} J^2$, where ρ_{FM} is the electrical resistivity of the ferromagnetic material (typically, permalloy with $\rho_{\mathrm{FM}} \approx 1 \times 10^{-7}$ Ωm) and V_{FM} is the volume of the magnetic nanowire. For a 200-nm-wide nanowire with a thickness of 5 nm and and a length of 10 μm, $P_{\mathrm{STT}} \approx 10$ mW. In multiferroic heterostructures, resistive Joule heating is very small due to the high electrical resistivity of ferroelectric materials ($\rho_{\mathrm{FE}} \approx 1 \times 10^9$ Ωm for $BaTiO_3$). An estimation based on $P_{\mathrm{E,Joule}} = V_{\mathrm{FE}} E^2 / \rho_{\mathrm{FE}}$ gives a heat dissipation of about 10 fW if the ferroelectric material is patterned to the same dimensions as the ferromagnetic nanowire. The primary source of power consumption in multiferroic heterostructures is therefore not given by Joule heating but by the ferroelectric switching process. For lateral ferroelectric domain-wall motion, it can be estimated by $P_E = P_{\mathrm{FE}} E A_{\mathrm{FE}} v_{\mathrm{FE}}$, where P_{FE} and A_{FE} are the polarization and cross section of the ferroelectric material ($P_{\mathrm{FE}} = 0.26$ C/m^2 for $BaTiO_3$), E is the applied electric field, and v_{FE} is the wall velocity. Domain-wall velocities of several hundred meters per second would require an electric field of the order of 100 kV/cm (extrapolation from data in Fig. 5). For a nanowire, the power dissipation would be about 1 μW. Power consumption of electric-field-driven magnetic domain-wall motion can thus be several orders of magnitude smaller than for current-based STT if multiferroic heterostructures are patterned to similar dimensions. Although nontrivial nanoscale effects need to be addressed in future investigations before such structures become feasible, the demonstrated ability to reversibly drive magnetic domain walls by electric fields only opens up interesting possibilities for the design of magnetic devices.

VI. CONCLUSION

Reversible electric-field-driven magnetic domain-wall motion is demonstrated for $Fe/BaTiO_3$ heterostructures. Strong elastic pinning of magnetic domain walls onto ferroelectric domain boundaries forms the basis of an all-electrical driving mechanism, which allows for accurate control over the position and velocity of magnetic domain walls. Reproducible back-and-forth motion of a magnetic domain wall is achieved by the use of a ferroelectric *a-c* domain boundary and out-of-plane electric-field pulses. Future experiments can build on these results by exploring various magnetic domain-wall structures and higher electric fields in patterned nanowires.

ACKNOWLEDGMENTS

We are thankful to T. H. E. Lahtinen and A. Casiraghi for fruitful discussions. This work was supported by the European Research Council (ERC-2012-StG 307502-E-CONTROL), the Industrial Technology Research Grant Program in 2009 from New Energy and Industrial Technology Development Organization (NEDO) of Japan, JSPS KAKENHI (Grant No. 24.7390), the Advanced Materials Development and Integration of Novel Structured Metallic and Inorganic Materials Project of MEXT, and the Collaborative Research Project of the Materials and Structures Laboratory, Tokyo Institute of Technology. K. J. A. F. acknowledges financial support from the Finnish Doctoral Program in Computational Sciences, and B. V. d. W. received financial support from the Flanders Research Foundation.

APPENDIX

The domain-wall pinning potential that is created in a ferromagnetic film through elastic coupling to a ferroelectric domain wall can be estimated by considering a lateral displacement of the magnetic domain-wall profile with respect to the ferroelectric boundary (see Fig. 7). In equilibrium, the magnetization profile of a domain wall $\phi(x)$ that separates two domains R_i ($i = 1, 2$) with different magnetic anisotropies is given by total energy minimization. If this wall profile is assumed to be constant, the pinning potential in zero magnetic field can be estimated by considering magnetic anisotropy only. For domains R_i exhibiting both uniaxial (K_{ui}) and cubic (K_{ci}) anisotropy, the energy density can be written as

$$e_i = K_{ui} \sin^2[\phi(x) - \theta_i] + K_{ci} \sin^2\{2[\phi(x) - \psi_i]\}, \qquad \text{(A1)}$$

where θ_i and ψ_i indicate the direction of the easy anisotropy axes with respect to the domain wall. Sideways motion of the magnetic domain-wall profile by a distance d away from the ferroelectric domain boundary increases the anisotropy energy of the system. The magnetic energy per unit domain-wall length for a ferromagnetic film of thickness t at a position d away from the ferroelectric boundary is given by

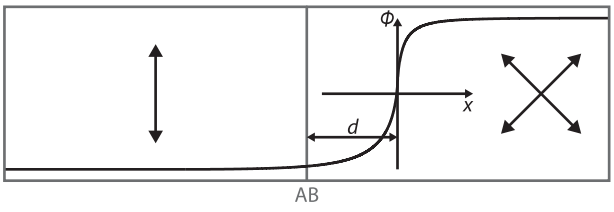

FIG. 7. The domain-wall pinning potential $V(d)$ of an anisotropy boundary (AB) between domains with uniaxial and cubic magnetic anisotropy can be estimated by calculating the increase of anisotropy energy when the magnetic domain wall $[\phi(x)]$ is moved to position d. The anisotropy boundary in the Fe film is created by elastic coupling to an underlying ferroelectric *a-c* domain wall in the $BaTiO_3$ substrate.

$$E(d)=t\int_{-\infty}^{-d}dxK_{u1}\sin^2[\phi(x)-\theta_1]+K_{c1}\sin^2\{2[\phi(x)-\psi_1]\} +t\int_{-d}^{\infty}dxK_{u2}\sin^2[\phi(x)-\theta_2]+K_{c2}\sin^2\{2[\phi(x)-\psi_2]\}. \tag{A2}$$

In our experimental system, domain R_1 corresponds to the uniaxial a domain with $\theta_1 = 0°$ and domain R_2 corresponds to the cubic c domain with $\psi_2 = 45°$. For this configuration, Eq. (A2) simplifies to

$$E(d) = t\int_{-\infty}^{-d}dxK_a\sin^2[\phi(x)] + t\int_{-d}^{\infty}dxK_c\cos^2[2\phi(x)]. \tag{A3}$$

The domain-wall pinning potential at position d is given by $V(d) = E(d) - E(0)$, i.e.,

$$V(d) = t\left[\int_{-\infty}^{-d}dxK_a\sin^2[\phi(x)] + \int_{-d}^{\infty}dxK_c\cos^2[2\phi(x)]\right] - t\left[\int_{-\infty}^{0}dxK_a\sin^2[\phi(x)]+\int_{0}^{\infty}dxK_c\cos^2[2\phi(x)]\right]. \tag{A4}$$

In our $Fe/BaTiO_3$ samples, $K_a = 2K_c$, which results in a nearly symmetric domain-wall pinning potential [see Fig. 1(c)].

[1] N. L. Schryer and L. R. Walker, *The Motion of 180° Domain Walls in Uniform dc Magnetic Fields*, J. Appl. Phys. **45**, 5406 (1974).

[2] L. Berger, *Exchange Interaction between Ferromagnetic Domain Wall and Electric Current in Very Thin Metallic Films*, J. Appl. Phys. **55**, 1954 (1984).

[3] T. Ono, H. Miyajima, K. Shigeto, K. Mibu, N. Hosoito, and T. Shinjo, *Propagation of a Magnetic Domain Wall in a Submicrometer Magnetic Wire*, Science **284**, 468 (1999).

[4] J. Grollier, P. Boulenc, V. Cros, A. Hamzić, A. Vaurès, A. Fert, and G. Faini, *Switching a Spin Valve Back and Forth by Current-Induced Domain Wall Motion*, Appl. Phys. Lett. **83**, 509 (2003).

[5] G. Tatara and H. Kohno, *Theory of Current-Driven Domain Wall Motion: Spin Transfer versus Momentum Transfer*, Phys. Rev. Lett. **92**, 086601 (2004).

[6] G. S. D. Beach, C. Nistor, C. Knutson, M. Tsoi, and J. L. Erskine, *Dynamics of Field-Driven Domain-Wall Propagation in Ferromagnetic Nanowires*, Nat. Mater. **4**, 741 (2005).

[7] A. Thiaville, Y. Nakatani, J. Miltat, and Y. Suzuki, *Micromagnetic Understanding of Current-Driven Domain Wall Motion in Patterned Nanowires*, Europhys. Lett. **69**, 990 (2005).

[8] M. Kläui, C. A. F. Vaz, J. A. C. Bland, W. Wernsdorfer, G. Faini, E. Cambril, L. J. Heyderman, F. Nolting, and U. Rüdiger, *Controlled and Reproducible Domain Wall Displacement by Current Pulses Injected into Ferromagnetic Ring Structures*, Phys. Rev. Lett. **94**, 106601 (2005).

[9] M. Hayashi, L. Thomas, Y. B. Bazaliy, C. Rettner, R. Moriya, X. Jiang, and S. S. P. Parkin, *Influence of Current on Field-Driven Domain Wall Motion in Permalloy Nanowires from Time Resolved Measurements of Anisotropic Magnetoresistance*, Phys. Rev. Lett. **96**, 197207 (2006).

[10] T. A. Moore, I. M. Miron, G. Gaudin, G. Serret, S. Auffret, B. Rodmacq, A. Schuhl, S. Pizzini, J. Vogel, and M. Bonfim, *High Domain Wall Velocities Induced by Current in Ultrathin* $Pt/Co/AlO_x$ *Wires with Perpendicular Magnetic Anisotropy*, Appl. Phys. Lett. **93**, 262504 (2008).

[11] W. Kleemann, *Universal Domain Wall Dynamics in Disordered Ferroic Materials*, Annu. Rev. Mater. Sci. **37**, 415 (2007).

[12] S. Lemerle, J. Ferré, C. Chappert, V. Mathet, T. Giamarchi, and P. Le Doussal, *Domain Wall Creep in an Ising Ultrathin Magnetic Film*, Phys. Rev. Lett. **80**, 849 (1998).

[13] U. Bauer, S. Emori, and G. S. D. Beach, *Electric Field Control of Domain Wall Propagation in* $Pt/Co/GdO_x$ *Films*, Appl. Phys. Lett. **100**, 192408 (2012).

[14] A. J. Schellekens, A. van den Brink, J. H. Franken, H. J. M. Swagten, and B. Koopmans, *Electric-Field Control of Domain Wall Motion in Perpendicularly Magnetized Materials*, Nat. Commun. **3**, 847 (2012).

[15] D. Chiba, M. Kawaguchi, S. Fukami, N. Ishiwata, K. Shimamura, K. Kobayashi, and T. Ono, *Electric-Field Control of Magnetic Domain-Wall Velocity in Ultrathin Cobalt with Perpendicular Magnetization*, Nat. Commun. **3**, 888 (2012).

[16] U. Bauer, S. Emori, and G. S. D. Beach, *Voltage-Gated Modulation of Domain Wall Creep Dynamics in an Ultrathin Metallic Ferromagnet*, Appl. Phys. Lett. **101**, 172403 (2012).

[17] E. Mikheev, I. Stolichnov, E. De Ranieri, J. Wunderlich, H. J. Trodahl, A. W. Rushforth, S. W. E. Riester, R. P. Campion, K. W. Edmonds, B. L. Gallagher, and N. Setter, *Magnetic Domain Wall Propagation under Ferroelectric Control*, Phys. Rev. B **86**, 235130 (2012).

[18] A. Bernand-Mantel, L. Herrera-Diez, L. Ranno, S. Pizzini, J. Vogel, D. Givord, S. Auffret, O. Boulle, I. M. Miron, and G. Gaudin, *Electric-Field Control of Domain Wall Nucleation and Pinning in a Metallic Ferromagnet*, Appl. Phys. Lett. **102**, 122406 (2013).

[19] J. H. Franken, Y. Yin, A. J. Schellekens, A. van den Brink, H. J. M. Swagten, and B. Koopmans, *Voltage-Gated Pinning in a Magnetic Domain-Wall Conduit*, Appl. Phys. Lett. **103**, 102411 (2013).

[20] Z. Huang, I. Stolichnov, A. Bernand-Mantel, J. Borrel, S. Auffret, G. Gaudin, O. Boulle, S. Pizzini, L. Ranno, L. Herrera Diez, and N. Setter, *Ferroelectric Control of Magnetic Domains in Ultra-thin Cobalt Layers*, Appl. Phys. Lett. **103**, 222902 (2013).

[21] N. Lei, T. Devolder, G. Agnus, P. Aubert, L. Daniel, J.-V. Kim, W. Zhao, T. Trypiniotis, R. P. Cowburn, C. Chappert, D. Ravelosona, and P. Lecoeur, *Strain-Controlled Magnetic Domain Wall Propagation in Hybrid Piezoelectric/Ferromagnetic Structures*, Nat. Commun. **4**, 1378 (2013).

[22] E. de Ranieri, P. E. Roy, D. Fang, E. K. Vehsthedt, A. C. Irvine, D. Heiss, A. Casiraghi, R. P. Campion, B. L. Gallagher, T. Jungwirth, and J. Wunderlich, *Piezoelectric Control of the Mobility of a Domain Wall Driven by Adiabatic and Non-adiabatic Torques*, Nat. Mater. **12**, 808 (2013).

[23] U. Bauer, L. Yao, A. J. Tan, P. Agrawal, S. Emori, H. L. Tuller, S. van Dijken, and G. S. D. Beach, *Magneto-Ionic Control of Interfacial Magnetism*, Nat. Mater. **14**, 174 (2015).

[24] T.-K. Chung, G. P. Carman, and K. P. Mohanchandra, *Reversible Magnetic Domain-Wall Motion under an Electric Field in a Magnetoelectric Thin Film*, Appl. Phys. Lett. **92**, 112509 (2008).

[25] D. E. Parkes, S. A. Cavill, A. T. Hindmarch, P. Wadley, F. McGee, C. R. Staddon, K. W. Edmonds, R. P. Campion, B. L. Gallagher, and A. W. Rushforth, *Non-volatile Voltage Control of Magnetization and Magnetic Domain Walls in Magnetostrictive Epitaxial Thin Films*, Appl. Phys. Lett. **101**, 072402 (2012).

[26] W. Eerenstein, N. D. Mathur, and J. F. Scott, *Multiferroic and Magnetoelectric Materials*, Nature (London) **442**, 759 (2006).

[27] R. Ramesh and N. A. Spaldin, *Multiferroics: Progress and Prospects in Thin Films*, Nat. Mater. **6**, 21 (2007).

[28] J. Ma, J. Hu, Z. Li, and C.-W. Nan, *Recent Progress in Multiferroic Magnetoelectric Composites: From Bulk to Thin Films*, Adv. Mater. **23**, 1062 (2011).

[29] C. A. F. Vaz, *Electric Field Control of Magnetism in Multiferroic Heterostructures*, J. Phys. Condens. Matter **24**, 333201 (2012).

[30] Y.-H. Chu, L. W. Martin, M. B. Holcomb, M. Gajek, S.-J. Han, Q. He, N. Balke, C.-H. Yang, D. Lee, W. Hu, Q. Zhan, P.-L. Yang, A. Fraile-Rodríguez, A. Scholl, S. X. Wang, and R. Ramesh, *Electric-Field Control of Local Ferromagnetism Using a Magnetoelectric Multiferroic*, Nat. Mater. **7**, 478 (2008).

[31] D. Lebeugle, A. Mougin, M. Viret, D. Colson, and L. Ranno, *Electric Field Switching of the Magnetic Anisotropy of a Ferromagnetic Layer Exchange Coupled to the Multiferroic Compound* $BiFeO_3$, Phys. Rev. Lett. **103**, 257601 (2009).

[32] T. H. E. Lahtinen, J. O. Tuomi, and S. van Dijken, *Pattern Transfer and Electric-Field-Induced Magnetic Domain Formation in Multiferroic Heterostructures*, Adv. Mater. **23**, 3187 (2011).

[33] J. T. Heron, M. Trassin, K. Ashraf, M. Gajek, Q. He, S. Y. Yang, D. E. Nikonov, Y.-H. Chu, S. Salahuddin, and R. Ramesh, *Electric-Field-Induced Magnetization Reversal in a Ferromagnet-Multiferroic Heterostructure*, Phys. Rev. Lett. **107**, 217202 (2011).

[34] R. V. Chopdekar, V. K. Malik, A. Fraile Rodríguez, L. Le Guyader, Y. Takamura, A. Scholl, D. Stender, C. W. Schneider, C. Bernhard, F. Nolting, and L. J. Heyderman, *Spatially Resolved Strain-Imprinted Magnetic States in an Artificial Multiferroic*, Phys. Rev. B **86**, 014408 (2012).

[35] R. Streubel, D. Köhler, R. Schäfer, and L. M. Eng, *Strain-Mediated Elastic Coupling in Magnetoelectric Nickel/Barium-Titanate Heterostructures*, Phys. Rev. B **87**, 054410 (2013).

[36] K. J. A. Franke, D. L. González, S. J. Hämäläinen, and S. van Dijken, *Size Dependence of Domain Pattern Transfer in Multiferroic Heterostructures*, Phys. Rev. Lett. **112**, 017201 (2014).

[37] K. J. A. Franke, T. H. E. Lahtinen, and S. van Dijken, *Field Tuning of Ferromagnetic Domain Walls on Elastically Coupled Ferroelectric Domain Boundaries*, Phys. Rev. B **85**, 094423 (2012).

[38] T. H. E. Lahtinen, K. J. A. Franke, and S. van Dijken, *Electric-Field Control of Magnetic Domain Wall Motion and Local Magnetization Reversal*, Sci. Rep. **2**, 258 (2012).

[39] T. H. E. Lahtinen, Y. Shirahata, L. Yao, K. J. A. Franke, G. Venkataiah, T. Taniyama, and S. van Dijken, *Alternating Domains with Uniaxial and Biaxial Magnetic Anisotropy in Epitaxial Fe Films on* $BaTiO_3$, Appl. Phys. Lett. **101**, 262405 (2012).

[40] X. Zhang, T. Hashimoto, and D. C. Joy, *Electron Holographic Study of Ferroelectric Domain Walls*, Appl. Phys. Lett. **60**, 784 (1992).

[41] J. Hlinka and P. Márton, *Phenomenological Model of a 90° Domain Wall in* $BaTiO_3$*-Type Ferroelectrics*, Phys. Rev. B **74**, 104104 (2006).

[42] Q. Zhang and W. A. Goddard, *Charge and Polarization Distributions at the 90° Domain Wall in Barium Titanate Ferroelectric*, Appl. Phys. Lett. **89**, 182903 (2006).

[43] T. Mitsui and J. Furuichi, *Domain Structure of Rochelle Salt and* KH_2PO_4, Phys. Rev. **90**, 193 (1953).

[44] A. K. Tagantsev, L. E. Cross, and J. Fousek, *Domains in Ferroic Crystals and Thin Films* (Springer, New York, 2010).

[45] H. L. Stadler and P. J. Zachmanidis, *Nucleation and Growth of Ferroelectric Domains in* $BaTiO_3$ *at Fields from 2 to* 450 kV/cm, J. Appl. Phys. **34**, 3255 (1963).

[46] A. Vansteenkiste and B. Van de Wiele, *MuMax: A New High-Performance Micromagnetic Simulation Tool*, J. Magn. Magn. Mater. **323**, 2585 (2011).

[47] B. Van de Wiele, L. Laurson, K. J. A. Franke, and S. van Dijken, *Electric Field Driven Magnetic Domain Wall Motion in Ferromagnetic-Ferroelectric Heterostructures*, Appl. Phys. Lett. **104**, 012401 (2014).

[48] J. Leliaert, B. Van de Wiele, A. Vansteenkiste, L. Laurson, G. Durin, L. Dupré, and B. Van Waeyenberge, *A Numerical Approach to Incorporate Intrinsic Material Defects in Micromagnetic Simulations*, J. Appl. Phys. **115**, 17D102 (2014).

[49] J.-S. Kim, O. Boulle, S. Verstoep, L. Heyne, J. Rhensius, M. Kläui, L. J. Heyderman, F. Kronast, R. Mattheis, C. Ulysse, and G. Faini, *Current-Induced Vortex Dynamics and Pinning Potentials Probed by Homodyne Detection*, Phys. Rev. B **82**, 104427 (2010).

[50] T. Y. Chen, M. J. Erickson, P. A. Crowell, and C. Leighton, *Surface Roughness Dominated Pinning Mechanism of Magnetic Vortices in Soft Ferromagnetic Films*, Phys. Rev. Lett. **109**, 097202 (2012).

[51] J. A. J. Burgess, A. E. Fraser, F. F. Sani, D. Vick, B. D. Hauer, J. P. Davis, and M. R. Freeman, *Quantitative Magneto-mechanical Detection and Control of the Barkhausen Effect*, Science **339**, 1051 (2013).